



Guaranteed prediction and estimation of the state of a road network

Alex A. Kurzhanskiy^{a,*}, Pravin Varaiya^b

^a California PATH, University of California, Berkeley, United States

^b Department of Electrical Engineering and Computer Science, University of California, Berkeley, United States

ARTICLE INFO

Article history:

Received 31 August 2010

Received in revised form 22 August 2011

Accepted 26 August 2011

Keywords:

Nonlinear filtering

Set-valued estimation

Prediction

Cell Transmission Model

Feedback control

Uncertainty

ABSTRACT

The paper presents an algorithm for the prediction and estimation of the state of a road network comprising freeways and arterials, described by a Cell Transmission Model (CTM). CTM divides the network into a collection of links. Each link is characterized by its fundamental diagram, which relates link speed to link density. The state of the network is the vector of link densities. The state is observed through measurements of speed and flow on some links. Demand is specified by the volume of vehicles entering the network at some links, and by split ratios according to which vehicles are routed through the network. There is model uncertainty: the parameters of the fundamental diagram are uncertain. There is uncertainty in the demand around the nominal forecast. Lastly, the measurements are uncertain. The uncertainty in each model parameter, demand, and measurement is specified by an interval. Given measurements over a time interval $[0, t]$ and a horizon $\tau \geq 0$, the algorithm computes a set of states with the guarantee that the actual state at time $(t + \tau)$ will lie in this set, consistent with the given measurements. In standard terminology the algorithm is a state prediction or an estimate accordingly as $\tau > 0$ or $= 0$. The flow exiting a link may be controlled by an open- or closed-loop controller such as a signal or ramp meter. An open-loop controller does not change the algorithm, indeed it may make the system more predictable by tightening density bounds downstream of the controller. In the feedback case, the value of the control depends on the estimated state bounds, and the algorithm is extended to compute the range of possible closed-loop control values. The algorithm is used in a proposed design of a decision support system for the I-80 integrated corridor.

© 2011 Elsevier Ltd. All rights reserved.

1. Introduction

Standard control theory provides a useful framework for formulating and answering questions of real time traffic management. In this framework the evolution of the road network traffic is modeled as a dynamical system,

$$x(t+1) = f(t, x(t), u(t), v(t)), \quad t \geq 0, \quad (1.1)$$

$$y(t) = h(t, x(t), w(t)), \quad (1.2)$$

in which $x(t)$ is the traffic state vector at time t . The evolution of $x(t)$ is affected by both controlled inputs (ramp metering, signal settings, changeable message signs) denoted by $u(t)$, and uncontrolled inputs or disturbances (demand, events, weather, incidents) denoted by $v(t)$. The vector $y(t)$ of detector measurements (flow, density, speed, incidents) provides information about the traffic state according to (1.2), in which $w(t)$ is the measurement ‘noise’. In the framework, the traffic management strategy is just a feedback function Φ

* Corresponding author.

E-mail addresses: akurzhan@eecs.berkeley.edu (A.A. Kurzhanskiy), varaiya@eecs.berkeley.edu (P. Varaiya).

$$u(t) = \Phi(t, y[0, t]),$$

which specifies how the control $u(t)$ is selected on the basis of the measurements available up to that time, namely $y[0, t] = \{y(s), s \leq t\}$.

Suppose we are given the road network model $\{f, h\}$, the feedback function Φ , and a probabilistic characterization of the uncertainties in the forecast demand, disturbances and measurement noise $\{v(t), w(t) | t \geq 0\}$. Then the prediction of the traffic state at a future time is summarized by the probability distribution of the future state, conditioned on the measurements available at the present time (Kumar and Varaiya, 1986). That is, the prediction of $x(t + \tau)$ is the function

$$\Psi(\xi, t + \tau, t, y[0, t]) = \text{Prob}(x(t + \tau) = \xi | y(s), 0 \leq s \leq t),$$

which is the probability density that $x(t + \tau) = \xi$, conditioned on the measurements $y[0, t]$. The function Ψ summarizes everything one can know about the road network performance under the specified feedback function or management strategy. For example, from Ψ one can calculate the average performance of the feedback function in terms (say) of the expected delay as well as the risk in terms (say) of its variance. As another example, from Ψ one can calculate the likelihood or probability of the event that congestion will develop during $[t, t + \tau]$. One can then determine whether a proposed management strategy provides adequate average performance and acceptable risk, or whether a proposed strategy improves upon the baseline strategy.

Two difficulties make it virtually impossible to calculate the function Ψ . The first difficulty is computational. To appreciate it, consider a 20 km long two-directional highway, with detectors every 500 m reporting speed and density every 30 s. Then $y(t)$ is a 160-dimensional vector. Suppose the freeway is modeled as a nonlinear discrete-space, discrete-time system, with 500 m links in each direction, with the state as the vector of link densities. Then $x(t)$ is a vector of dimension 80. So Ψ is the probability distribution of the 80-dimensional vector $x(t + \tau)$ which depends on the $80 \times t$ -dimensional measurements $y[0, t]$. Computing Ψ is at present impossible. However, with sufficient computational resources, one may be able to calculate more or less satisfactory approximations to Ψ , although to our knowledge no one has attempted to do this calculation. Much more commonly, one resorts to an approximate calculation of the expected value of $x(t)$, conditional on $y[0, t]$, with no attempt to calculate the risk or dispersion of the distribution around this point estimate. As a consequence, one cannot estimate performance measures, such as travel time or delay, which are nonlinear function of the density.

The second difficulty may be more fundamental. The calculation of Ψ assumes that f, g, Φ and the probability distributions of the demand forecast errors, disturbances and measurement errors, are accurately known. This assumption, however, does not hold in practice. The assumed models and probability distributions will have specification errors which must be accounted for in the prediction Ψ . One possible move that overcomes this difficulty is to parameterize the unknown specification errors in a (large) parameter vector θ , place a prior distribution on θ , and augment (1.1) with the additional state vector $\theta(t)$, with

$$\theta(t + 1) = \theta(t).$$

The prediction function is correspondingly augmented:

$$\Psi(\xi, \theta, t + \tau, t, y[0, t]) = \text{Prob}(x(t + \tau) = \xi, \theta(t + \tau) = \theta | y(s), 0 \leq s \leq t).$$

The computation of this function is thereby much more difficult, and makes this standard control theory formulation more impractical.

Previous work on the traffic state estimation and prediction using macroscopic traffic models consists of variations on the theme of Kalman Filter and Monte Carlo methods. In (Sun et al., 2003), a piecewise linear replacement of the CTM is introduced and the Mixture Kalman Filter (MKF) is used to estimate the discrete and continuous state of the system. In (Tampère and Immers, 2007) the Extended Kalman Filter (EKF) framework for freeway traffic state estimation presented in (Wang and Papageorgiou, 2007) was applied to CTM. The Uncented Kalman Filter (UKF) (Julier et al., 2000), which overcomes some disadvantages of EKF, such as the need for linearization and complicated calculations of Jacobians and Hessians, was compared to EKF in (Hegyi et al., 2006), and it was concluded that their performance was comparable. Particle Filter (PF) approach and its comparison to UKF is described in (Mihaylova et al., 2007). These stochastic filtering techniques rely on assumptions about distributions of the inputs (MKF, EKF), or require large number of simulations to get reasonable result from Monte Carlo methods (UKF, PF): for example, the system with K uncertain inputs and no parametric uncertainty would require a minimum of 2^K simulations to reasonably represent the distribution of the system state.

We propose a different approach for traffic state prediction and estimation, based on set-valued (or bounding) philosophy (Kurzhanski, 1972, 1989; Milanese et al., 1996), that is computationally feasible. We incorporate all of the probabilistic and modeling uncertainty in a (large) parameter vector γ and rewrite the dynamical system as a deterministic system with an unknown uncertainty parameter γ :

$$x(t + 1) = f(t, x(t), u(t), \gamma), \tag{1.3}$$

$$y(t) = h(t, x(t), \gamma). \tag{1.4}$$

We assume that we have prior knowledge that the unknown γ belongs to a known set Γ . Instead of the probability distribution Ψ we now seek to find sets $X(t + \tau, t, y[0, t])$ such that, consistent with the measurements $y[0, t]$, we can guarantee that

$$x(t + \tau) \in X(t + \tau, t, y[0, t]), \text{ for all } \gamma \in \Gamma. \tag{1.5}$$

We call X a (set-valued) *guaranteed prediction*. With a guaranteed prediction, we can calculate guaranteed upper and lower bounds on system performance. Note that whereas the prediction Ψ tells us the likelihood that the state $x(t + \tau) = \xi$, guaranteed prediction only tells us that $x(t + \tau) = \xi$ for some $\xi \in X(t + \tau, t, y[0, t])$. By convention, X is called a predictor (estimator) when $\tau > 0 (=0)$.

The usefulness of guaranteed prediction depends on the answer to two questions. Q1: How ‘tight’ is the guaranteed prediction relative to possible behaviors of (1.3) and (1.4)? Q2: How difficult is it to compute a guaranteed prediction?

There is one obvious answer to Q1: the set $\widehat{X}(t + \tau, t, y[0, t])$ comprising all $x(t + \tau)$ that can be attained by a trajectory of (1.3) for some $\gamma \in \Gamma$ such that $h(s, x(s), \gamma)$, $s \in [0, t]$, agrees with the given measurements $y[0, t]$, is the smallest possible guaranteed prediction satisfying (1.5). This is simply a consistency condition. Unfortunately, calculating the set \widehat{X} that satisfies this consistency condition is extremely difficult; moreover, the computational complexity will grow with t .

To make this calculation of acceptable difficulty we look for a *recurrent* prediction. We wish that $X(t + \tau + 1, t, y[0, t])$ can be calculated from $X(t + \tau, t, y[0, t])$ and that $X(t + \tau, t + 1, y[0, t + 1])$ can be calculated from $X(t + \tau, t, y[0, t])$ and the new measurement $y(t + 1)$. The algorithm to calculate (1.5) will be recursive, its complexity will be bounded independently of t , and one can use it for online prediction.

In the succeeding sections we consider the Cell Transmission Model (CTM) of a road network of freeways and signalized arterials. We will take the parameter vector γ to comprise the uncertainties in the link fundamental diagrams, the demand forecast and the measurements. These uncertainties will be specified by intervals:

$$\Gamma = \{ \gamma = (\gamma_i) | \gamma_i \in [\bar{\gamma}_i - \epsilon_i^-, \bar{\gamma}_i + \epsilon_i^+] \}.$$

Thus Γ is a ‘box’ of parameter vector, surrounding the nominal vector $\bar{\gamma} = (\bar{\gamma}_i)$. The guaranteed prediction that we provide is also a box. In some special cases, it will turn out that the guaranteed prediction is the best possible, i.e., it coincides with \widehat{X} .

This work was inspired by the behavior analysis of CTM in (Gomes et al., 2008). It extends the set-valued estimation method of (Kurzhanskiy et al., 2009) for freeways and significantly improves the prediction/estimation result of (Kurzhanskiy and Varaiya, 2010) for road networks by exploiting the properties of the underlying dynamical model. We also pay special attention to the impact of the feedback control on the state prediction.

The rest of the paper is organized as follows. Section 2 introduces notation and formulates the underlying dynamical traffic model. Section 3 defines the uncertainty in the system parameters and inputs, explains the assumptions about the measurements, and sets up the problems of guaranteed traffic state prediction and estimation. Section 4 presents the state prediction algorithm and explores its properties. State estimation as a prediction–correction process is covered in Section 5. Section 6 addresses the impact of the closed-loop control on the prediction algorithm. Section 7 illustrates the use of guaranteed prediction in a real time decision support system for the I-80 integrated corridor management. Finally, Section 8 provides a conclusion.

2. Dynamical traffic model

We start by introducing the Cell Transmission Model (Daganzo, 1994; Daganzo, 1995). The road network consists of directed links and nodes: links represent stretches of roads and nodes connect the links. Denote by \mathcal{L} the set of links, and by \mathcal{N} the set of nodes in the network. A node must always have at least one input and at least one output link. A link is called an

Table 1
Model parameters and variables.

Symbol	Description	Value	Unit
Δx_l	Length of link $l \in \mathcal{L}$	$\in [0.05, 0.2]$	Miles
Δt	Size of time step	$\in [\frac{1}{3600}, \frac{1}{360}]$	Hours
F_l	Capacity of link $l \in \mathcal{L}$	for 1 lane $\in [1500, 2000]$	Vehicles per hour
v_l	Free flow speed in link $l \in \mathcal{L}$	For freeways $\in [60, 75]$ For arterials $\in [25, 40]$	Miles per hour
w_l	Congestion wave speed in link $l \in \mathcal{L}$	$\in [5, 20]$	Miles per hour
ρ_l	Jam density in link $l \in \mathcal{L}$	For 1 lane $\in [160, 210]$	Vehicles per mile
ρ_l^c	Critical density in link $l \in \mathcal{L}$	For 1 lane $\in [20, 50]$	Vehicles per mile
t	Time	$\in [0, \infty]$	Hours
$B_v(t)$	Split ratio matrix in node $v \in \mathcal{N}$	$\beta_{ij}(t) \in [0, 1], \sum_j \beta_{ij}(t) = 1$	Dimensionless
$r_l(t)$	Demand at origin link $l \in \mathcal{L}$	Variable	Vehicles per hour
$f_l^u(t)$	Flow entering link $l \in \mathcal{L}$	Variable	Vehicles per hour
$f_l^d(t)$	Flow exiting link $l \in \mathcal{L}$	Variable	Vehicles per hour
$V_l(t)$	Traffic speed in link $l \in \mathcal{L}$	Variable	Miles per hour
$\rho_l(t)$	Vehicle density in link $l \in \mathcal{L}$	Variable	Vehicles per mile
$\rho(t)$	Vector of densities in all links in \mathcal{L}	Variable	Vehicles per mile
$C(t, \rho)$	Control that restricts flow out of link l	Variable	Vehicles per hour

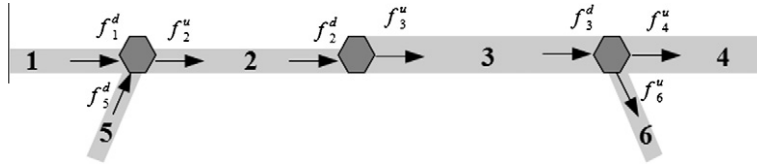


Fig. 1. Simple road network – links are numbered from 1 to 6, nodes are shown in dark gray.

ordinary link, if it has both begin and end nodes. A link with no begin node is an *origin*, and a link with no end node is a *destination*.

Table 1 lists the model variables and parameters with plausible values. Each link $l \in \mathcal{L}$ is characterized by its length Δx_l , and the triangular fundamental diagram defined by capacity F_l , free flow speed v_l , and congestion wave speed w_l (or alternatively, by F_l , ρ_l^c , and $\bar{\rho}_l$). F_l takes into account the number of lanes. Origins are the links through which vehicles enter the system, and therefore have demand profiles $r_l(\cdot)$ assigned to them. Each node $v \in \mathcal{N}$ is characterized by a split ratio matrix \mathcal{B}_v , that determines how the incoming flows are distributed among the output links. Nodes may be used not only to represent intersections, merge, or diverge points, but also to break up long links into smaller ones.

In the simple example of a single-directional freeway of Fig. 1, nodes are places where on-ramps merge into and off-ramps diverge from the freeway, or where freeway characteristics, such as the fundamental diagram, change; ordinary links are the stretches of freeway going from node to node; origins are on-ramps; and destinations are off-ramps.

The state of the road network at time t consists of the vehicle density in each link, $\rho_l(t)$. Given some initial condition, which usually comes from measurements, $\rho_l(t_0) = \rho_l^0$, the system evolves in time according to

$$\rho_l(t + \Delta t) = \rho_l(t) + \frac{\Delta t}{\Delta x_l} (f_l^u(t) - f_l^d(t)) \text{ for each } l \in \mathcal{L}, \tag{2.1}$$

where Δt must satisfy $\Delta t \leq \min_l \left\{ \frac{\Delta x_l}{v_l} \right\}$ and $\Delta t \leq \min_l \left\{ \frac{\Delta x_l}{w_l} \right\}$.¹ For origins, $f_l^u(t) = r_l(t)$, where $r_l(t)$ is the demand – the flow that desires to enter the system through origin l at time t . For destinations, $f_l^d(t) = v_l \rho_l(t) \min \left\{ 1, \frac{F_l}{v_l \rho_l(t)} \right\}$. For ordinary links, $f_l^u(t)$ is determined by the begin or upstream node and $f_l^d(t)$ is determined by the end or downstream node of link l .

The node v with m input and n output links has the $m \times n$ split ratio matrix $\mathcal{B}_v(t) = \{\beta_{ij}(t)\}_{i=1, \dots, m}^{j=1, \dots, n}$. This matrix is nonnegative and the sum of the elements in each row equals 1. $\beta_{ij}(t)$ is the portion of the vehicle flow coming from input link i that has to be directed to output link j at time t . Input flows $f_i^d(t)$ and output flows $f_j^u(t)$, $i = 1, \dots, m$, $j = 1, \dots, n$, for the node are computed in steps 1–7 that follow.²

1. Compute available supply for each output link:

$$s_j(t) = \min \left\{ F_j, w_j (\bar{\rho}_j - \rho_j(t)) \right\}, j = 1, \dots, n, \tag{2.2}$$

where F_j is the capacity, w_j is the congestion wave speed, $\bar{\rho}_j$ is the jam density, and $\rho_j(t)$ is the current density of output link j .

2. Set iteration $p = 0$. (Below, $p = 1, \dots, n$ will index output links.)
3. Compute demands from each input link:

$$d_i^{[0]}(t) = v_i \rho_i(t) \min \left\{ 1, \frac{F_i}{v_i \rho_i(t)}, \frac{C_i(t, \boldsymbol{\rho})}{v_i \rho_i(t)} \right\}, i = 1, \dots, m, \tag{2.3}$$

where F_i is the capacity, v_i is the free flow speed, $\rho_i(t)$ is the current density of the input link i , and $C_i(t, \boldsymbol{\rho})$ represents a controller function, e.g., ramp meter, variable speed limit, signal, potentially restricting the flow from link i . Observe that this permits formulating both open-loop ($C_i(t, \boldsymbol{\rho})$ not depending on $\boldsymbol{\rho}$) as well as traffic responsive control. If there is no flow control in link i , $C_i(t, \boldsymbol{\rho}) = \infty$. Quantity $d_i^{[0]}(t)$ represents the flow desiring to exit input link i , restricted by the control, but not yet restricted by the output links.

4. Compute output demands:

¹ This necessary condition for convergence while solving hyperbolic PDEs numerically is known as Courant–Friedrichs–Lewy (CFL) condition (Courant et al., 1928).

² In this paper we use the node model of Aurora Road Network Modeler (Kurzhanskiy et al., 2009; Aurora RNM Homepage, n.d.), which is similar to the node model of (Jin and Zhang, 2003 and Bliemer, 2007). Depending on the structure of split ratio matrix the proposed node model performs better or worse than that of (Bliemer, 2007) in terms of maximization of the total output flow. It was shown in (Tampère et al., 2011), however, that these node models may be overly conservative in restricting the output flow, in some cases violating the invariance principle of (Lebacque and Khoshyaran, 2005), and a more robust node model was proposed instead. In most node configurations, however, namely, freeway merges (m -to-1) or diverges (1-to- n) and arterial intersections modeled as in (Chow et al., 2010), where incoming flows do not compete for the downstream supply because of being assigned to conflicting signal phases, the proposed node model maximizes the output flow subject to the upstream demand, downstream supply and the first-in-first-out rule restrictions.

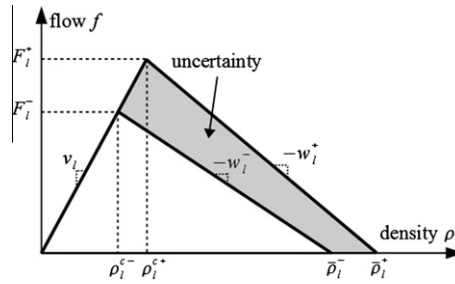


Fig. 2. Uncertainty in the fundamental diagram of link $l \in \mathcal{L}$.

$$d_j^{*[p]}(t) = \sum_{i=1}^m \beta_{ij}(t) d_i^{[p]}(t), j = 1, \dots, n. \tag{2.4}$$

Quantity $d_j^{*[0]}(t)$ represents the total flow that desires to enter the output link j .

5. For $p = 1, \dots, n$, and for each input link $i, i = 1, \dots, m$, repeat
 - (a) scale down input demand to satisfy the output supply if necessary:

$$d_i^{[p]}(t) = \begin{cases} d_i^{[p-1]}(t), & \text{if } \beta_{ip}(t) = 0 \\ d_i^{[p-1]}(t) \min \left\{ 1, \frac{s_p(t)}{d_i^{[p-1]}(t)} \right\}, & \text{otherwise;} \end{cases} \tag{2.5}$$

- (b) if $p < n$, recompute output demand $d_{p+1}^{*[p]}(t)$ according to (2.4).
This step implements the proportional priority rule for merging links (Jin and Zhang, 2003), and the first-in-first-out rule for diverging links as stated in (Daganzo, 1995).³

6. Flow leaving the input link i is

$$f_i(t)^d = d_i^{[n]}(t), i = 1, \dots, m. \tag{2.6}$$

7. Flow entering the output link j is

$$f_j^u(t) = \sum_{i=1}^m \beta_{ij}(t) d_i^{[n]}(t), j = 1, \dots, n. \tag{2.7}$$

Given the initial condition $t = t_0, \rho(t_0) = \rho_0$, at each time step of the system evolution $t(t \geq t_0)$, first the input and output flows for each node $v \in \mathcal{N}$ are computed using steps 1–7 above, and then the system state is updated via the conservation Eq. (2.1).

3. Problem statement

Traffic state estimation and prediction requires knowledge of the initial conditions, inputs (demands) and system parameters. Initial conditions can be derived from incoming real-time traffic measurements. Future demands cannot be known exactly, but several approaches are available to estimate them using historical measurement data, such as (Lin, 2001; Okutani and Stephanedes, 1984; Smith et al., 2002). System parameters, i.e., fundamental diagrams and split ratio matrices, can also be obtained from the historical data. (Of course, the Δx_l are known exactly, and the time step Δt is chosen based on values of Δx_l and $v_l, l \in \mathcal{L}$.) Estimating capacity and calibrating the fundamental diagrams is addressed in (Dervisoglu et al., 2009). Empirical data show that measurements on the free flow side of the fundamental diagram are well represented by a straight line, whereas measurements in the congested region are scattered (Dervisoglu et al., 2009; Kurzhanskiy and Varaiya, 2010; Muralidharan et al., 2011). In particular, in (Muralidharan et al., 2011) it is stated that freeway measurement data analysis indicates no significant variations in free flow speed, and while capacity and congestion speed both vary noticeably, the impact of capacity variation is much stronger than that of congestion speed variation. Using maximum daily flow measurements from a traffic database such as PeMS (PeMS Homepage, n.d.), we can construct a box plot describing the capacity variation for each detector station in our road network, similar to the one in Fig. 4 of (Muralidharan et al., 2011). Then, F_l^- and F_l^+ can be defined as lower and upper quartiles of the box plot for the corresponding link l . For marterials it is safe to assume that the free flow speed equals the speed limit, jam density can be reliably estimated, but it is difficult to measure the capacity. Thus, in this paper we assume both the capacity and congestion wave speed to be uncertain.

³ Proportional priority rule means that each output link accommodates vehicles from the input links in proportion to the input demands. First-in-first-out rule means that the input-to-output flows in the node should always be in proportion to each other as defined by the split ratio matrix.

We assume that demands $r_l(t)$ at origin links are estimated or forecast with uncertainty expressed by intervals $r_l^-(t) \leq r_l(t) \leq r_l^+(t)$ ($r_l^-(t)$ and $r_l^+(t)$ are known)⁴; link capacities F_l and jam densities $\bar{\rho}_l, l \in \mathcal{L}$, lie within given intervals $F_l^- \leq F_l \leq F_l^+$ (F_l^- and F_l^+ are known) and $\bar{\rho}_l^- \leq \bar{\rho}_l \leq \bar{\rho}_l^+$ ($\bar{\rho}_l^-$ and $\bar{\rho}_l^+$ are known). Consequently $w_l^- \leq w_l \leq w_l^+$, with

$$w_l^- = \frac{F_l^-}{\bar{\rho}_l^- - F_l^- / v_l} \text{ and } w_l^+ = \frac{F_l^+}{\bar{\rho}_l^+ - F_l^+ / v_l},$$

We assume that the free flow speeds v_l are known exactly. Fig. 2 illustrates the uncertainty in the fundamental diagram. It is assumed that split ratio matrices $\mathcal{B}_v(t), v \in \mathcal{N}$, are known exactly.⁵ For now, we shall also assume that the traffic flow control function from expression (2.3) is known, and depends only on the time but not the state, i.e., $C_l(t, \rho) = C_l(t)$ (the control is open-loop). The case of known feedback traffic flow control is considered in Section 6.

There is additive ‘noise’ in measurements of the output flow

$$y_l^{(f)}(t) = f_l^d(t) + \omega_l^{(f)}(t), \tag{3.1}$$

and speed

$$y_l^{(v)}(t) = V_l(t) + \omega_l^{(v)}(t), \tag{3.2}$$

in each link. Here $\omega_l^{(f)}(t) \in [-\omega_l^{0,(f)}(t), \omega_l^{0,(f)}(t)]$ is the flow measurement noise, $\omega_l^{(v)}(t) \in [-\omega_l^{0,(v)}(t), \omega_l^{0,(v)}(t)]$ is the speed measurement noise; the bounds $\omega_l^{0,(f)}(t)$ and $\omega_l^{0,(v)}(t)$ are known. Thus, for each link we get an estimate of the density from the measurements alone:

$$\hat{\rho}_l^-(t) \leq \hat{\rho}_l(t) \leq \hat{\rho}_l^+(t), \tag{3.3}$$

with

$$\hat{\rho}_l^-(t) = \frac{y_l^{(f)}(t) - \omega_l^{0,(f)}(t)}{y_l^{(v)}(t) + \omega_l^{0,(v)}(t)} \text{ and } \hat{\rho}_l^+(t) = \frac{y_l^{(f)}(t) + \omega_l^{0,(f)}(t)}{y_l^{(v)}(t) - \omega_l^{0,(v)}(t)}. \tag{3.4}$$

The problems we intend to solve can now be succinctly stated.

- 1. Guaranteed traffic state prediction.** Find curves $\rho^-(\cdot)$ (the best case) and $\rho^+(\cdot)$ (the worst case) such that the trajectory of the system (2.1)–(2.7) with above specified demand and fundamental diagram uncertainties, $\rho(\cdot)$, is bounded as

$$\rho_l^-(t) \leq \rho_l(t) \leq \rho_l^+(t), \quad t \geq t_0, \tag{3.5}$$

for all $l \in \mathcal{L}$, where t_0 is the initial (current) time. By ‘best (worst) case’ we mean the smallest (largest) density, and by ‘curve’ we mean a function of time t .

- 2. Guaranteed traffic state estimation.** At given time instants $t_0 < \tau_1 < \tau_2 < \dots < \tau_k < \dots$, for each link $l \in \mathcal{L}$, the measurement bounds $[\hat{\rho}_l^-(\tau), \hat{\rho}_l^+(\tau)]$ (if measurements are available) are received. Compute prediction bounds $[\rho_l^-(\tau_1), \rho_l^+(\tau_1)]$, from the initial conditions at t_0 , and use the measurement bounds at time τ_1 to correct them; then use the corrected prediction bounds as new initial conditions for computing the prediction from τ_1 to τ_2 , and at time τ_2 perform the measurement correction again; and so on for $\tau = \tau_3, \dots, \tau_k, \dots$. At any given time $t \geq t_0$, the estimates for the system state are the prediction bounds corrected by measurements.

Remark. The term *guaranteed* is borrowed from the control theory (Kurzhanski, 1972, 1989; Milanese et al., 1996). It means that the current system state lies within calculated worst and best case bounds given that our assumptions about parameter (fundamental diagram) and input (demand) uncertainty, as well as measurement noise are *correct*.

4. Guaranteed traffic state prediction

Recalling the conservation Eq. (2.1), define the state update equation for density bounds:

$$\rho_l^\pm(t + \Delta t) = \rho_l^\pm(t) + \frac{\Delta t}{\Delta x_l} (f_l^{u^\pm}(t) - f_l^{d^\pm}(t)) \text{ for each } l \in \mathcal{L}. \tag{4.1}$$

⁴ Traffic measurement databases such as PeMS (PeMS Homepage, n.d.), allows us to construct time series of input flow data. For each origin link, we can take several time series without significant structural differences and obtain bounding curves $r_l^-(\cdot), r_l^+(\cdot)$ for them. Generally, it is observed that the same weekdays have repeating demand patterns. Thus, historic Monday demand data should be used for future Monday demand forecast, historic Tuesday demand data – for future Tuesday demand forecast, and so on. In real time, the forecasted demand bounds $r_l^\pm(\cdot)$ should be continuously corrected by the incoming flow measurements at origin links.

⁵ It is important to note that split ratio matrices must be well defined. Although it is possible to extend the result of the current paper to the case when split ratios are specified within intervals, or depend on the state of the system, such extension is beyond the scope of this work.

Table 2
Parameters and variables for model with uncertainty.

Symbol	Description	Unit
F_l^-	Lower capacity bound of link $l \in \mathcal{L}$	Vehicles per hour
F_l^+	Upper capacity bound of link $l \in \mathcal{L}$	Vehicles per hour
$\bar{\rho}_l^-$	Lower jam density bound in link $l \in \mathcal{L}$	Vehicles per mile
$\bar{\rho}_l^+$	Upper jam density bound in link $l \in \mathcal{L}$	Vehicles per mile
w_l^-	Congestion wave speed in link $l \in \mathcal{L}$ corresponding to F_l^- and $\bar{\rho}_l^-$	Miles per hour
w_l^+	Congestion wave speed in link $l \in \mathcal{L}$ corresponding to F_l^+ and $\bar{\rho}_l^+$	Miles per hour
$r_l^-(t)$	Best case (lower) demand bound at origin link $l \in \mathcal{L}$	Vehicles per hour
$r_l^+(t)$	Worst case (upper) demand bound at origin link $l \in \mathcal{L}$	Vehicles per hour
$f_l^{u-}(t)$	Best case flow bound entering link $l \in \mathcal{L}$	Vehicles per hour
$f_l^{u+}(t)$	Worst case flow bound entering link $l \in \mathcal{L}$	Vehicles per hour
$f_l^{d-}(t)$	Best case flow bound exiting link $l \in \mathcal{L}$	Vehicles per hour
$f_l^{d+}(t)$	Worst case flow bound exiting link $l \in \mathcal{L}$	Vehicles per hour
$\rho_l^-(t)$	Best case (lower) predicted density bound in link $l \in \mathcal{L}$	Vehicles per mile
$\rho_l^+(t)$	Worst case (upper) predicted density bound in link $l \in \mathcal{L}$	Vehicles per mile
$\boldsymbol{\rho}^-(t)$	Vector of best case (lower) density bounds in all links in \mathcal{L}	Vehicles per mile
$\boldsymbol{\rho}^+(t)$	Vector of worst case (upper) density bounds in all links in \mathcal{L}	Vehicles per mile
$\hat{\rho}_l^-(t)$	Lower measured density bound in link $l \in \mathcal{L}$	Vehicles per mile
$\hat{\rho}_l^+(t)$	Upper measured density bound in link $l \in \mathcal{L}$	Vehicles per mile

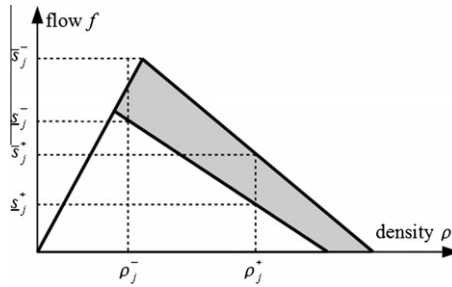


Fig. 3. Supply bounds for $f_j^{u-}(t)$ and $f_j^{u+}(t)$.

Any equation like the above involving the ‘±’ symbol in superscripts represents two separate equations, with ‘−’ for the lower (best case) bound, and ‘+’ for the upper (worst case) bound calculation. As before, Δt satisfies the CFL condition $\Delta t \leq \min_l \left\{ \frac{\Delta x_l}{v_l} \right\}$ and $\Delta t \leq \min_l \left\{ \frac{\Delta x_l (\bar{\rho}_l^- - F_l^- / v_l)}{F_l^-} \right\}$. For origin links, $f_l^{u\pm}(t) = r_l^\pm(t)$. For destination links, $f_l^{d-}(t) = v_l \rho_l^-(t) \min \left\{ 1, \frac{F_l^-}{v_l \rho_l^-(t)} \right\}$, and $f_l^{d+}(t) = v_l \rho_l^+(t) \min \left\{ 1, \frac{F_l^+}{v_l \rho_l^+(t)} \right\}$. For ordinary links, $f_l^{u\pm}(t)$ are determined by its begin node, and $f_l^{d\pm}(t)$ by its end node.

Table 2 summarizes newly introduced notation.

For a general node $v \in \mathcal{N}$ with m input, n output links, and split ratio matrix $\mathcal{B}_v(t) = \{\beta_{ij}(t)\}_{i=1, \dots, m}^{j=1, \dots, n}$, the incoming flows $f_i^{d\pm}, i = 1, \dots, m$, and outgoing flows $f_j^{u\pm}, j = 1, \dots, n$, are computed using the following algorithm.⁶

1. For each output link $j, j = 1, \dots, n$, compute the lower bounds of supply:

$$s_j^\pm(t) = \min \left\{ F_j^-, \max \left\{ 0, w_j^- \left(\bar{\rho}_j^- - \rho_j^\pm(t) \right) \right\} \right\}, \tag{4.2}$$

and the upper bounds of supply:

$$\bar{s}_j^\pm(t) = \min \left\{ F_j^+, w_j^+ \left(\bar{\rho}_j^+ - \rho_j^\pm(t) \right) \right\}. \tag{4.3}$$

From (4.2) and (4.3) it follows that $s_j^\pm(t) \leq \bar{s}_j^\pm(t)$, $s_j^+(t) \leq \bar{s}_j^-(t)$ and $\bar{s}_j^+(t) \leq \bar{s}_j^-(t)$. Fig. 3 illustrates what the values $s_j^\pm(t)$ and $\bar{s}_j^\pm(t)$ represent. We need to ensure that $s_j^+(t) \geq 0$, since it is possible that $\rho_j^+(t) > \bar{\rho}_j^-$. (Hence the 0 in (4.2).)

⁶ Implementing the guaranteed prediction algorithm for the node model of (Tampère et al., 2011) is the subject of future research.

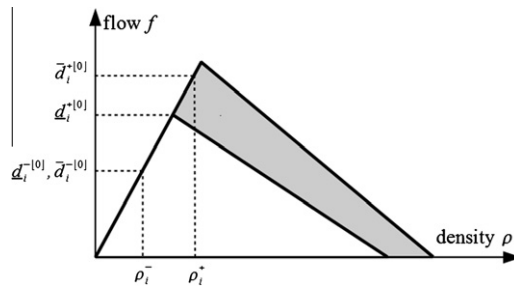


Fig. 4. Demand bounds for $f_i^{d-}(t)$ and $f_i^{d+}(t)$.

2. Set iteration $p = 0$.

3. For each input link $i, i = 1, \dots, m$, compute the lower bounds of demand:

$$\underline{\delta}_i^{\pm[0]}(t) = \underline{d}_i^{\pm[0]}(t) = v_i \rho_i^{\pm}(t) \min \left\{ 1, \frac{F_i^-}{v_i \rho_i^{\pm}(t)}, \frac{C_i(t)}{v_i \rho_i^{\pm}(t)} \right\}, \quad (4.4)$$

and the bounds of demand:

$$\bar{\delta}_i^{\pm[0]}(t) = \bar{d}_i^{\pm[0]}(t) = v_i \rho_i^{\pm}(t) \min \left\{ 1, \frac{F_i^+}{v_i \rho_i^{\pm}(t)}, \frac{C_i(t)}{v_i \rho_i^{\pm}(t)} \right\}. \quad (4.5)$$

From (4.4), (4.5) it follows that $\underline{d}_i^{\pm[0]}(t) \leq \bar{d}_i^{\pm[0]}(t)$, $\underline{d}_i^{-[0]}(t) \leq \underline{d}_i^{+[0]}(t)$ and $\bar{d}_i^{-[0]}(t) \leq \bar{d}_i^{+[0]}(t)$. Fig. 4 illustrates what the values $\underline{d}_i^{\pm[0]}(t)$ and $\bar{d}_i^{\pm[0]}(t)$ represent.

4. For each output link $j, j = 1, \dots, n$, compute output demand lower bounds:

$$\underline{d}_j^{* \pm [p]}(t) = \sum_{i=1}^m \beta_{ij}(t) \underline{d}_i^{\pm [p]}(t), \quad (4.6)$$

and upper bounds:

$$\bar{d}_j^{* \pm [p]}(t) = \sum_{i=1}^m \beta_{ij}(t) \bar{d}_i^{\pm [p]}(t). \quad (4.7)$$

Evidently, $\underline{d}_i^{* \pm [0]}(t) \leq \bar{d}_i^{* \pm [0]}(t)$, $\underline{d}_i^{* - [0]}(t) \leq \underline{d}_i^{* + [0]}(t)$ and $\bar{d}_i^{* - [0]}(t) \leq \bar{d}_i^{* + [0]}(t)$.

5. For $p = 1, \dots, n$, and for each input link $i, i = 1, \dots, m$, repeat

(a) scale down the best case auxiliary upper input demand bound $\bar{d}_i^{-[p]}(t)$ to satisfy the best case upper supply bound $\bar{s}_p^-(t)$:

$$\bar{d}_i^{-[p]}(t) = \begin{cases} \bar{d}_i^{-[p-1]}(t), & \text{if } \beta_{ip}(t) = 0 \\ \bar{d}_i^{-[p-1]}(t) \min \left\{ 1, \frac{\bar{s}_p^-(t)}{\bar{d}_i^{-[p-1]}(t)} \right\}, & \text{otherwise;} \end{cases} \quad (4.8)$$

(b) scale down the worst case auxiliary lower input demand bound $\underline{d}_i^{+[p]}(t)$ to satisfy the worst case lower supply bound $s_p^+(t)$:

$$\underline{d}_i^{+[p]}(t) = \begin{cases} \underline{d}_i^{+[p-1]}(t), & \text{if } \beta_{ip}(t) = 0 \\ \underline{d}_i^{+[p-1]}(t) \min \left\{ 1, \frac{s_p^+(t)}{\underline{d}_i^{+[p-1]}(t)} \right\}, & \text{otherwise;} \end{cases} \quad (4.9)$$

(c) scale down the best case upper input demand bound $\bar{\delta}_i^{-[p]}(t)$ to satisfy the best case upper supply bound $\bar{s}_p^-(t)$:

$$\bar{\delta}_i^{-[p]}(t) = \begin{cases} \bar{\delta}_i^{-[p-1]}(t), & \text{if } \beta_{ip}(t) = 0 \\ \bar{\delta}_i^{-[p-1]}(t) \min \left\{ 1, \max \left\{ \frac{\bar{s}_p^-(t)}{\bar{d}_i^{-[p-1]}(t)}, \frac{s_p^+(t)}{\underline{d}_i^{+[p-1]}(t)} \right\} \right\}, & \text{otherwise;} \end{cases} \quad (4.10)$$

(d) scale down the worst case lower input demand bound $\bar{\delta}_i^{-[p]}(t)$ to satisfy the worst case lower supply bound $\underline{s}_p^+(t)$:

$$\underline{\delta}_i^{+[p]}(t) = \begin{cases} \bar{\delta}_i^{+[p-1]}(t), & \text{if } \beta_{ip}(t) = 0 \\ \bar{\delta}_i^{+[p-1]}(t) \min \left\{ 1, \frac{\underline{s}_p^+(t)}{\underline{d}_p^{+[p-1]}(t)}, \frac{\bar{s}_p^-(t)}{\bar{d}_p^{+[p-1]}(t)} \right\}, & \text{otherwise;} \end{cases} \quad (4.11)$$

(e) if $p < n$, recompute the best case upper output demand bounds $\bar{d}_{p+1}^{+-[p]}(t)$ according to (4.7) and the worst case lower output demand bounds $\underline{d}_{p+1}^{+-[p]}(t)$ according to (4.6).

6. For each input link $i, i = 1, \dots, m$, the best case flow leaving the link is

$$f_i^{d-}(t) = \bar{\delta}_i^{-[n]}(t), \quad (4.12)$$

and the worst case flow leaving the link is

$$f_i^{d+}(t) = \underline{\delta}_i^{+[n]}(t). \quad (4.13)$$

7. For each output link $j, j = 1, \dots, n$, repeat

(a) for $p = 1, \dots, n$ repeat

i. scale down the best case lower input demand bound $\underline{d}_i^{-[p]}(t)$ to satisfy the worst case lower supply bound $\underline{s}_p^+(t)$ for $p \neq j$, and the best case lower supply bound $\underline{s}_j^-(t)$ for $p = j$:

$$\underline{d}_i^{-[p]}(t) = \begin{cases} \bar{d}_i^{-[p-1]}(t), & \text{if } \beta_{ip}(t) = 0 \\ \bar{d}_i^{-[p-1]}(t) \min \left\{ 1, \frac{\underline{s}_p^+(t)}{\underline{d}_p^{-[p-1]}(t)} \right\}, & \text{if } \beta_{ip} > 0 \text{ and } p \neq j \\ \bar{d}_i^{-[p-1]}(t) \min \left\{ 1, \frac{\underline{s}_j^-(t)}{\underline{d}_p^{-[p-1]}(t)} \right\}, & \text{if } \beta_{ip} > 0 \text{ and } p = j; \end{cases} \quad (4.14)$$

This is a step in computation of the best case incoming flow for the output link j . So, the corresponding demand bound $\underline{d}_i^{-[p]}(t)$ is scaled down to satisfy the best case lower supply bound only for the output link j , whereas for the other output links it is scaled down even more – to satisfy the worst case lower supply bounds.

ii. Scale down the worst case upper input demand bound $\bar{d}_i^{+[p]}(t)$ to satisfy the best case upper supply bound $\bar{s}_p^-(t)$: for $p \neq j$, and the worst case upper supply bound $\bar{s}_j^+(t)$ for $p = j$:

$$\bar{d}_i^{+[p]}(t) = \begin{cases} \underline{d}_i^{+[p-1]}(t), & \text{if } \beta_{ip}(t) = 0 \\ \underline{d}_i^{+[p-1]}(t) \min \left\{ 1, \frac{\bar{s}_p^-(t)}{\bar{d}_p^{+[p-1]}(t)} \right\}, & \text{if } \beta_{ip} > 0 \text{ and } p \neq j \\ \underline{d}_i^{+[p-1]}(t) \min \left\{ 1, \frac{\bar{s}_j^+(t)}{\bar{d}_p^{+[p-1]}(t)} \right\}, & \text{if } \beta_{ip} > 0 \text{ and } p = j; \end{cases} \quad (4.15)$$

This is a step in computation of the worst case incoming flow for the output link j . So, the corresponding demand bound $\bar{d}_i^{+[p]}(t)$ is scaled down to satisfy the worst case upper supply bound only for the output link j , whereas for the other output links it is scaled down less – to satisfy the best case upper supply bounds.

iii. Recompute the best case lower output demand bounds $\underline{d}_{p+1}^{+-[p]}(t)$ according to (4.6) and the worst case upper output demand bounds $\bar{d}_{p+1}^{+-[p]}(t)$ according to (4.7);

(b) the best case flow entering the link is

$$f_j^{u-}(t) = \sum_{i=1}^m \beta_{ij}(t) \underline{d}_i^{-[n]}(t), \quad (4.16)$$

and the worst case flow entering the link is

$$f_j^{u+}(t) = \min \left\{ \bar{s}_j^+(t), \sum_{i=1}^m \beta_{ij}(t) \bar{d}_i^{+[n]}(t) \right\}. \quad (4.17)$$

Given the initial conditions $t = t_0, \rho^-(t_0) = \rho_0^-$ and $\rho^+(t_0) = \rho_0^+$, such that $\rho_l^-(t_0) \leq \rho_l^+(t_0)$ for all $l \in \mathcal{L}$,⁷ at each time step of the prediction system evolution $t(t \geq t_0)$ we (1) compute $f_l^{u\pm}(t)$ and $f_l^d(t)^\pm$ using steps 1–7 for all $l \in \mathcal{L}$, and (2) update the density bounds $\rho_l^\pm(t+1)$ using (4.1) for all $l \in \mathcal{L}$. The following facts describe the properties of the constructed system (4.1)–(4.17).

⁷ The initial density bounds may come from the measurement (3.4) or previous state estimation.

Theorem 4.1. *If the initial conditions $\rho_l^-(t_0) = \rho_l^+(t_0)$, and there is no uncertainty in demands ($r_l^-(t) = r_l^+(t), t \geq t_0$) and fundamental diagrams ($F_l^- = F_l^+, \bar{\rho}_l^- = \bar{\rho}_l^+$), for all $l \in \mathcal{L}$, then $\rho^-(\cdot) = \rho^+(\cdot) = \rho(\cdot)$, where $\rho(\cdot)$ is a trajectory of system 2.1, 2.2, 2.3, 2.4, 2.5, 2.6, 2.7.*

Proof. The proof is a direct consequence of the fact that $s_j^-(t) = s_j^+(t) = \bar{s}_j^-(t) = \bar{s}_j^+(t), j = 1, \dots, n$, and $\underline{d}_i^{\pm[0]}(t) = \underline{d}_i^{+[0]}(t) = \bar{d}_i^{\pm[0]}(t) = \bar{d}_i^{+[0]}(t) i = 1, \dots, m$, where $s_j^\pm(t), \bar{s}_j^\pm(t)$ are defined in (4.2) and (4.3), and $\underline{d}_i^{\pm[0]}(t), \bar{d}_i^{\pm[0]}(t)$ are defined in (4.4) and (4.5). \square

Theorem 4.2 (Monotonicity). *System 4.1, 4.2, 4.3, 4.4, 4.5, 4.6, 4.7, 4.8, 4.9, 4.10, 4.11, 4.12, 4.13, 4.14, 4.15, 4.16, 4.17 preserves partial order: if $\rho_l^-(t_0) \leq \rho_l^+(t_0)$ for each $l \in \mathcal{L}$, then $\rho_l^-(t) \leq \rho_l^+(t)$ for each $l \in \mathcal{L}$ and any $t \geq t_0$.*

Proof. Suppose, at some time $t \geq t_0$ $\rho_l^-(t) \leq \rho_l^+(t)$ for all $l \in \mathcal{L}$. We must show that for any $l \in \mathcal{L}, \rho_l^-(t + \Delta t), \rho_l^+(t + \Delta t)$ obtained from (4.1)–(4.17) satisfy $\rho_l^-(t + \Delta t) \leq \rho_l^+(t + \Delta t)$. From (4.1) we get

$$\rho_l^+(t + \Delta t) - \rho_l^-(t + \Delta t) = \rho_l^+(t) - \rho_l^-(t) + \frac{\Delta t}{\Delta x_l} (f_l^{u+}(t) - f_l^{u-}(t) + f_l^{d-}(t) - f_l^{d+}(t)).$$

We shall consider three cases.

Case 1: $\rho_l^-(t) \leq \rho_l^+(t) \leq \rho_l^{c-} = \frac{F_l^-}{v_l}$.
 Since $f_l^{u-}(t) \leq f_l^{u+}(t)$,

$$\begin{aligned} \rho_l^+(t + \Delta t) - \rho_l^-(t + \Delta t) &\geq \rho_l^+(t) - \rho_l^-(t) - \frac{\Delta t}{\Delta x_l} (f_l^{d+}(t) - f_l^{d-}(t)) \geq \rho_l^+(t) - \rho_l^-(t) - \frac{\Delta t}{\Delta x_l} (v_l \rho_l^+(t) - v_l \rho_l^-(t)) \\ &= (\rho_l^+(t) - \rho_l^-(t)) \left(1 - \frac{v_l \Delta t}{\Delta x_l} \right) \geq \left\{ \text{CFL condition : } 1 \geq \frac{v_l \Delta t}{\Delta x_l} \right\} \geq 0. \end{aligned}$$

Case 2: $\rho_l^{c-} \leq \rho_l^-(t) \leq \rho_l^+(t)$.
 Since $f_l^{d-}(t) \geq f_l^{d+}(t)$,

$$\begin{aligned} \rho_l^+(t + \Delta t) - \rho_l^-(t + \Delta t) &\geq \rho_l^+(t) - \rho_l^-(t) - \frac{\Delta t}{\Delta x_l} (f_l^{u-}(t) - f_l^{u+}(t)) \\ &\geq \rho_l^+(t) - \rho_l^-(t) - \frac{\Delta t}{\Delta x_l} (w_l^-(\bar{\rho}_l^- - \rho_l^-(t)) - w_l^+(\bar{\rho}_l^+ - \rho_l^+(t))) \\ &\geq \rho_l^+(t) - \rho_l^-(t) - \frac{\Delta t}{\Delta x_l} (w_l^+(\bar{\rho}_l^+ - \rho_l^-(t)) - w_l^+(\bar{\rho}_l^+ - \rho_l^+(t))) = (\rho_l^+(t) - \rho_l^-(t)) \left(1 - \frac{w_l^+ \Delta t}{\Delta x_l} \right) \\ &\geq \left\{ \text{CFL condition : } 1 \geq \frac{w_l^+ \Delta t}{\Delta x_l} \right\} \geq 0. \end{aligned}$$

Case 3: $\rho_l^-(t) \leq \rho_l^{c-} \leq \rho_l^+(t)$.
 Since $f_l^{u-} \leq F_l^-$ and $f_l^{d+}(t) \leq F_l^-$,

$$\begin{aligned} \rho_l^+(t + \Delta t) - \rho_l^-(t + \Delta t) &\geq \rho_l^+(t) - \rho_l^-(t) - \frac{\Delta t}{\Delta x_l} (F_l^- - f_l^{u+}(t) + F_l^- - f_l^{d-}(t)) \geq \\ \rho_l^+(t) - \rho_l^-(t) - \frac{\Delta t}{\Delta x_l} (F_l^- - w_l^+(\bar{\rho}_l^+ - \rho_l^+(t)) + F_l^- - v_l \rho_l^-(t)) &= \\ \rho_l^+(t) - \rho_l^{c-} + \rho_l^{c-} - \rho_l^-(t) - \frac{\Delta t}{\Delta x_l} (w_l^-(\bar{\rho}_l^- - \rho_l^{c-}) - w_l^+(\bar{\rho}_l^+ - \rho_l^+(t)) + v_l \rho_l^c - v_l \rho_l^-(t)) &\geq \\ \rho_l^+(t) - \rho_l^{c-} + \rho_l^{c-} - \rho_l^-(t) - \frac{\Delta t}{\Delta x_l} (w_l^+(\bar{\rho}_l^+ - \rho_l^{c-}) - w_l^+(\bar{\rho}_l^+ - \rho_l^+(t)) + v_l \rho_l^c - v_l \rho_l^-(t)) &= \\ (\rho_l^+(t) - \rho_l^{c-}) \left(1 - \frac{w_l^+ \Delta t}{\Delta x_l} \right) + (\rho_l^{c-} - \rho_l^-(t)) \left(1 - \frac{v_l \Delta t}{\Delta x_l} \right) &\geq \\ \left\{ \text{CFL condition : } 1 \geq \frac{w_l^+ \Delta t}{\Delta x_l} \text{ and } 1 \geq \frac{v_l \Delta t}{\Delta x_l} \right\} &\geq 0. \quad \square \end{aligned}$$

Theorem 4 shows that the trajectory of the system (4.1)–(4.17) is a *box-valued tube*: at each time $t \geq t_0$ the state of this system is a box

$$\Omega(t) = \{ \tilde{\rho} | \rho_l^-(t) \leq \tilde{\rho}_l \leq \rho_l^+(t), \forall l \in \mathcal{L} \}. \tag{4.18}$$

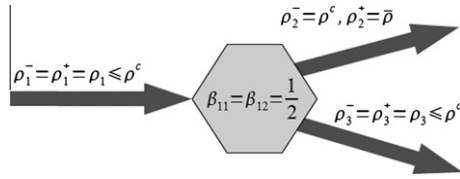


Fig. 5. Simple network – a node with 1 input and 2 output links.

From Theorem 4 follows the next statement.

Corollary 4.1 (Theorem of two policemen). Any trajectory $\rho(\cdot)$ of system 2.1, 2.2, 2.3, 2.4, 2.5, 2.6, 2.7 with uncertain demands and fundamental diagrams satisfies $\rho^-(\cdot) \leq \rho(\cdot) \leq \rho^+(\cdot)$,⁸ or $\rho(t) \in \Omega(t)$ for $t \geq t_0$.

This corollary means that $\Omega(t)$ is an overapproximation of the reachable set for system (2.1)–(2.7) with given uncertainty in demands and fundamental diagrams. Hence $\Omega(t)$ is a guaranteed prediction. Note that the computation of $\Omega(t)$ is recurrent and only requires solving the two Eq. (4.1). We now explore the tightness of this overapproximation.

Theorem 4.3 (System in free flow). If $f_l^{d+}(t) = v_l \rho_l^+(t)$ for all $l \in \mathcal{L}$ and $t \geq t_0$, then $\rho^-(\cdot)$ and $\rho^+(\cdot)$ are trajectories of system 2.1, 2.2, 2.3, 2.4, 2.5, 2.6, 2.7 with demands $r_l^-(t)$ and $r_l^+(t)$ at origin links respectively.

Proof. The proof follows from the fact that $\underline{d}_i^{\pm[0]}(t) = \bar{d}_i^{\pm[0]}(t)$ where $\underline{d}_i^{\pm[0]}(t)$ and $\bar{d}_i^{\pm[0]}(t)$ are defined in (4.4) and (4.5) respectively; and the fact that $\underline{d}_i^{\pm[p]}(t) = \bar{d}_i^{\pm[p]}(t) = \underline{d}_i^{\pm[p-1]}(t) = \bar{d}_i^{\pm[p-1]}(t)$ for $p = 1, \dots, n$, in (4.10), (4.11), (4.14) and (4.15). □

The intuition behind this theorem is that if even the worst case density bounds are in the free flow region, the uncertainty in the fundamental diagrams plays no role in the system dynamics. Theorem 4.3 shows that if the road network is in free flow, the prediction box $\Omega(t), t \geq t_0$, defined in (4.18) is the smallest box containing the reachable set of the system (2.1)–(2.7) with given uncertainty in demands and fundamental diagrams. This tightness in prediction of the system state in free flow is important because it yields a more accurate detection of the initial congestion. Another interpretation of Theorem 4.3 is that in free flow the system 2.1, 2.2, 2.3, 2.4, 2.5, 2.6, 2.7 is monotone.

If at some time $t \geq t_0$ there exists a link l whose desired worst case exiting flow exceeds its lower capacity bound ($v_l \rho_l^+(t) \geq F_l$) or downstream supply, the curves $\rho^-(\cdot)$ and $\rho^+(\cdot)$ are not necessarily trajectories of the system (2.1)–(2.7). The following example illustrates this fact, showing also that the system (2.1)–(2.7) is not monotone.

Example. Consider the road network comprising a single node with 1 input and 2 output links, depicted in Fig. 5. All three links have the same fundamental diagram without uncertainty: $F_1 = F_2 = F_3 = F$; $v_1 = v_2 = v_3 = v$; and $w_1 = w_2 = w_3 = w$ ($\rho^c_1 = \rho^c_2 = \rho^c_3 = \rho^c$ and $\bar{\rho}_1 = \bar{\rho}_2 = \bar{\rho}_3 = \bar{\rho}$). The initial conditions at time $t_0 = 0$ are $\rho_l^{\pm}(0) = \rho_l^{\pm}$, $l = 1, 2, 3$, where $\rho_1^- = \rho_1^+ = \rho_1 \leq \rho^c$, $\rho_2^- = \rho^c$, $\rho_2^+ = \bar{\rho}$ and $\rho_3^- = \rho_3^+ = \rho_3 \leq \rho^c$; and no flow is entering link 1. Split ratio matrix at the node is $B = \begin{bmatrix} \frac{1}{2} & \frac{1}{2} \end{bmatrix}$. We also assume that $\Delta x_1 = \Delta x_2 = \Delta x_3 = 1$ mile.

First, we compute the state of system (4.1)–(4.17) at time $t = \Delta t, \Omega(\Delta t) = \{\bar{\rho} | \rho^-(\Delta t) \leq \bar{\rho} \leq \rho^+(\Delta t)\}$:

$$\rho^-(\Delta t) = \begin{pmatrix} \rho_1 - v\rho_1\Delta t \\ \rho^c - (F - \frac{1}{2}v\rho_1)\Delta t \\ \rho_3 - v\Delta t\rho_3 \end{pmatrix} \text{ and } \rho^+(\Delta t) = \begin{pmatrix} \rho_1 \\ \bar{\rho} - F\Delta t; \\ \rho_3 - v\Delta t(\rho_3 - \frac{1}{2}\rho_1) \end{pmatrix}.$$

Then, we compute the states of system (2.1)–(2.7) with initial conditions $\rho_{\star}(0) = [\rho_1 \rho^c \rho_3]^T$ and $\rho^{\star}(0) = [\rho_1 \bar{\rho} \rho_3]^T$ at time $t = \Delta t$:

$$\rho_{\star}(\Delta t) = \begin{pmatrix} \rho_1 - v\rho_1\Delta t \\ \rho^c - (F - \frac{1}{2}v\rho_1)\Delta t \\ \rho_3 - v\Delta t(\rho_3 - \frac{1}{2}\rho_1) \end{pmatrix} \text{ and } \rho^{\star}(\Delta t) = \begin{pmatrix} \rho_1 \\ \bar{\rho} - F\Delta t; \\ \rho_3 - v\Delta t\rho_3 \end{pmatrix}.$$

If $\rho_1 > 0$, vectors $\rho_{\star}(\Delta t)$ and $\rho^{\star}(\Delta t)$ cannot be ordered, because although $\rho_{l\star}(\Delta t) \leq \rho_l^{\star}(\Delta t), l = 1, 2, \rho_{3\star}(\Delta t) > \rho_3^{\star}(\Delta t)$, which confirms that system (2.1)–(2.7) is not monotone. At the same time, both $\rho_{\star}(\Delta t)$ and $\rho^{\star}(\Delta t)$ are bounded by $\rho^-(\Delta t)$ and $\rho^+(\Delta t): \rho^-(\Delta t) \leq \rho_{\star}(\Delta t), \rho^{\star}(\Delta t) \leq \rho^+(\Delta t)$.

The quality of the proposed traffic state prediction mechanism depends on the time horizon (the shorter, the better), and the sizes of the uncertainty intervals (the larger the interval sizes, the less predictable is the system). In the studies of California freeways conducted within TOPL research project (TOPL Project, n.d.), we use 2-h prediction time horizon, and measurement data from PeMS (PeMS Homepage, n.d.) to construct capacity box plots and interval time series describing the demand. We observed that it is the uncertainty in the fundamental diagrams that affects the prediction results the most. The

⁸ For vectors $a, b \in \mathbb{R}^N$, expression “ $a \leq b$ ” means that component-wise a is less or equal to b : $a_k \leq b_k, k = 1, \dots, N$.

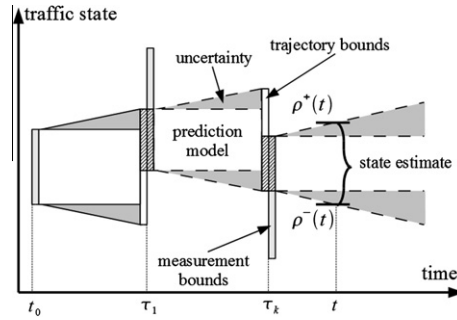


Fig. 6. Illustration of the traffic state estimation algorithm.

reason is that when the system state approaches the lower bound of the critical density, ρ_l^- ends up on the free flow side of the fundamental diagram, while ρ_l^+ ends up on its congested side, and if the difference between ρ_l^{c-} and ρ_l^{c+} is large enough, bounds ρ_l^- and ρ_l^+ can grow apart very fast. Thus, if the original maximum daily flow measurements produce prohibitively large capacity spread, we filter them by eliminating days with incidents and days with significantly different traffic patterns (e.g. if we model a weekday, we exclude weekends and vice versa).

5. Guaranteed traffic state estimation

The guaranteed estimation algorithm combines the guaranteed prediction (4.1)–(4.17) with measurement corrections (3.3) and (3.4) coming at times $t_0 < \tau_1 < \tau_2 < \dots < \tau_k < \dots$.

1. At time $\tau_0 = t_0$ generate measurement bounds $\hat{\rho}_l^-(\tau_0), \hat{\rho}_l^+(\tau_0)$ according to (3.4) for all $l \in \mathcal{L}$.
2. Assign

$$\rho_l^-(\tau_0) = \hat{\rho}_l^-(\tau_0) \text{ and } \rho_l^+(\tau_0) = \hat{\rho}_l^+(\tau_0) \quad (5.1)$$

for all $l \in \mathcal{L}$.

3. For $k = 1, 2, \dots$, repeat

- (a) compute $\rho_l^-(\tau_k)$ and $\rho_l^+(\tau_k)$ using (4.1)–(4.17) with initial conditions $\rho_l^-(\tau_{k-1}), \rho_l^+(\tau_{k-1})$ for all $l \in \mathcal{L}$;
- (b) acquire measurement bounds $\hat{\rho}_l^-(\tau_k), \hat{\rho}_l^+(\tau_k)$ according to (3.4) for all $l \in \mathcal{L}$;
- (c) presuming that

$$[\rho_l^-(\tau_k), \rho_l^+(\tau_k)] \cap [\hat{\rho}_l^-(\tau_k), \hat{\rho}_l^+(\tau_k)] \neq \emptyset, \quad (5.2)$$

perform measurement correction:

$$\rho_l^-(\tau_k) \leftarrow \max \{ \rho_l^-(\tau_k), \hat{\rho}_l^-(\tau_k) \} \text{ and } \rho_l^+(\tau_k) \leftarrow \min \{ \rho_l^+(\tau_k), \hat{\rho}_l^+(\tau_k) \} \quad (5.3)$$

for all $l \in \mathcal{L}$.

At any time $t \geq t_0$, the density estimate for link $l \in \mathcal{L}$ is the interval $[\rho_l^-(t), \rho_l^+(t)]$, and if $t = \tau_k$, $\rho_l^-(\tau_k), \rho_l^+(\tau_k)$ are presumed after the correction (5.3).

Fig. 6 illustrates the estimation algorithm: for every $k = 1, 2, \dots$ the trajectory of the system (4.1)–(4.17) is computed from τ_{k-1} to τ_k , then it is intersected with the measurement, and the result of this intersection serves as new initial condition. If a measurement occurs every time step, there is a prediction–correction at each step.

Non-emptiness of the interval Section (5.2) must be true in principle; otherwise, it would mean that we made wrong assumptions about the range of uncertainty. In practice, however, empty intersections do occur. What to do in case condition (5.2) is not satisfied, depends on the specific situation. If we trust our model more than the measurements, we should skip the correction (5.3). Moreover, we can use the dynamical model (4.1)–(4.17) to detect faulty measurement devices. If, on the other hand, we believe that, although an outlier, the measurement data are reliable, the measurement bounds should be used as initial conditions for the next prediction period, modifying the correction (5.3) as

$$\rho_l^-(\tau_k) \leftarrow \hat{\rho}_l^-(\tau_k), \text{ and } \rho_l^+(\tau_k) \leftarrow \hat{\rho}_l^+(\tau_k). \quad (5.4)$$

It is possible that for some links in \mathcal{L} the measurements do not exist or cannot be obtained. For such links, the correction (5.3) is skipped. The observability problem (what if the flow is measured but not the speed, or vice versa) is addressed in (Kurzhanskiy, 2009).

The quality of the proposed estimation technique depends on the spatial density of the healthy detector measurements. In the absence of measurements, any traffic state estimation attempt is as inadequate as a random guess. If there are too few

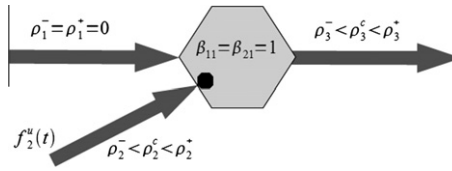


Fig. 7. Simple network – a node with 2 input and 1 output links.

measurements, the proposed method will produce a gap between the best and the worst cases that may be too large to be of use. The second important factor is the quality of the prediction discussed earlier – obviously, the shorter the interval between the measurement corrections, the smaller is the estimation interval.

6. Impact of feedback control

The controller that restricts the vehicle flow leaving link $l \in \mathcal{L}$ is modeled by the function $C_l(t, \rho)$: recall expressions (2.3), (4.4) and (4.5). In case of the open-loop control (time of day ramp metering, fixed timing plans for signalized intersections, etc.), function $C_l(t, \rho) = C_l(t)$ produces a single number at time t . For a node with m inputs and n outputs, if there exists an input link $i \in \{1, \dots, m\}$ such that $C_i(t) < F_i^+$, the interval size of $[\underline{\delta}_i^{\pm[0]}(t), \bar{\delta}_i^{\pm[0]}(t)]$ from (4.4) and (4.5) is reduced, which can potentially reduce the interval size of $[\rho_j^-(t + \Delta t), \rho_j^+(t + \Delta t)]$, $j = 1, \dots, n$, making the state in the downstream links more predictable.

In real time, when the system (4.1)–(4.17) is used as dynamical filter for the measurements, we know exactly the flow rates assigned by the controllers no matter whether these controllers are open- or closed-loop, and thus, the closed-loop control makes no difference in computation of $\rho^-(\cdot)$ and $\rho^+(\cdot)$. The situation is different, however, when the system (4.1)–(4.17) is used for prediction. Then, in the closed-loop case we do not know the values of $C_l(t, \rho)$, because, as was mentioned in Section 4, all we know about $\rho(t)$ is that it belongs to a box-valued set $\Omega(t)$ defined in (4.18) for each $t \geq t_0$.

Define

$$C_l^-(t, \Omega(t)) = \min_{\rho \in \Omega(t)} \{C_l(t, \tilde{\rho})\} \text{ and } C_l^+(t, \Omega(t)) = \max_{\rho \in \Omega(t)} \{C_l(t, \tilde{\rho})\}. \tag{6.1}$$

Formulas (4.4) and (4.5) from step 3 of the algorithm in Section 4 must be modified as follows:

$$\underline{\delta}_i^{\pm[0]}(t) = \underline{d}_i^{\pm[0]}(t) = v_i \rho_i^{\pm}(t) \min \left\{ 1, \frac{F_i^-}{v_i \rho_i^{\pm}(t)}, \frac{C_i^-(t, \Omega(t))}{v_i \rho_i^{\pm}(t)} \right\} \tag{6.2}$$

and

$$\bar{\delta}_i^{\pm[0]}(t) = \bar{d}_i^{\pm[0]}(t) = v_i \rho_i^{\pm}(t) \min \left\{ 1, \frac{F_i^+}{v_i \rho_i^{\pm}(t)}, \frac{C_i^+(t, \Omega(t))}{v_i \rho_i^{\pm}(t)} \right\} \tag{6.3}$$

for every input link $i = 1, \dots, m$. Just as (4.4) and (4.5), formulas (6.2) and (6.3) guarantee that $\underline{\delta}_i^{\pm[0]}(t) \leq \bar{\delta}_i^{\pm[0]}(t)$, $\underline{\delta}_i^{-[0]}(t) \leq \bar{\delta}_i^{-[0]}(t)$ and $\bar{\delta}_i^{-[0]}(t) \leq \bar{\delta}_i^{+[0]}(t)$.

Note that definition (6.1) cannot be replaced with

$$C_l^-(t, \Omega(t)) = \min \{C_l(t, \rho^-(t)), C_l(t, \rho^+(t))\} \text{ and } C_l^+(t, \Omega(t)) = \max \{C_l(t, \rho^-(t)), C_l(t, \rho^+(t))\},$$

since function $C_l(t, \rho)$ is not necessarily monotone in ρ . The next example explains this fact.

Example. Consider the road network comprising a single node with 2 input and 1 output links, shown in Fig. 7. All three links have fundamental diagrams without uncertainty: $F_l^- = F_l^+$ and $w_l^- = w_l^+(\rho_l^{c-} = \rho_l^{c+})$, and $\bar{\rho}_l^- = \bar{\rho}_l^+$, $l = 1, 2, 3$. The initial conditions at time $t_0 = 0$ are $\rho_l^{\pm}(0) = \rho_l^{\pm}$, $l = 1, 2, 3$, where $\rho_1^- = \rho_1^+ = 0$, $\rho_2^- = 0$, $\rho_2^+ > \rho_2^c$ and $\rho_3^- < \rho_3^c$, $\rho_3^+ > \rho_3^c$; no flow is entering link 1, and flow $f_2^d(t)$ is entering link 2.

Suppose, the traffic flow coming from the input link 2 is metered using the ALINEA algorithm (Papageorgiou et al., 1991). ALINEA is an example of a closed-loop control function defined by the formula

$$A_2(t, \rho_3(t)) = v_3(\rho_3^c - \rho_3(t)) + \begin{cases} f_2^d(t), & \text{if } t = 0 \\ A_2(t - \Delta t, \rho_3(t - \Delta t)), & \text{otherwise,} \end{cases} \tag{6.4}$$

where subscripts ‘2’ and ‘3’ refer to links 2 and 3 respectively, and A_2 is the ALINEA flow rate.

Let us compute the range of ALINEA flow rates for $t = 0$. Since $A_2(t, \rho_3)$ is monotone in ρ_3 , for $C_2(t, \rho(t)) = A_2(t, \rho_3(t))$ formula (6.1) at $t = 0$ translates into

$$C_2^-(0, \Omega(0)) = A_2(0, \rho_3^+) \text{ and } C_2^+(0, \Omega(0)) = A_2(0, \rho_3^-).$$

It is possible, however, for a controller such as ALINEA to work in conjunction with a queue controller that prevents the vehicle queue from growing too much, causing traffic spillback further upstream. The most common queue controller uses the queue override algorithm:

$$Q_2(t, \rho_2(t)) = f_2^u(t) + v_2(\rho_2(t) - \rho_2^c), \tag{6.5}$$

where Q_2 is the flow rate prescribed by the queue override controller. With both ALINEA and queue override active at the same time, the controller flow rate is computed as

$$C_2(t, \rho(t)) = \max \{A_2(t, \rho_3(t)), Q_2(t, \rho_2(t))\}, \tag{6.6}$$

which for $t = 0$ yields

$$C_2(0, \rho^-(0)) = A_2(0, \rho_3^-) = f_2^u(0) + v_3(\rho_3^c - \rho_3^-)$$

and

$$C_2(0, \rho^+(0)) = Q_2(0, \rho_2^+) = f_2^u(0) + v_2(\rho_2^+ - \rho_2^c).$$

Now we fix $\tilde{\rho}(0) = [0 \ \rho_2^- \ \rho_3^+]^T$. Obviously, $[0 \ \rho_2^- \ \rho_3^+]^T = \rho^-(0) \preceq \tilde{\rho}(0) \preceq \rho^+(0) = [0 \ \rho_2^+ \ \rho_3^+]^T$. That is, $\tilde{\rho}(0) \in \Omega(0)$. Following formula (6.6),

$$C_2(0, \tilde{\rho}(0)) = A_2(0, \tilde{\rho}(0)) = f_2^u(0) + v_3(\rho_3^c - \rho_3^+) < \min \{C_2(0, \rho^-(0)), C_2(0, \rho^+(0))\}.$$

Although in this paper we assume the split ratio matrices to be well defined and do not consider the case when their values depend on the traffic state, the described above treatment of the closed-loop control gives us a hint about the way of handling the state dependent split ratios.

7. Decision support system

Fig. 8 situates the guaranteed traffic state estimation and prediction algorithm within a proposed design of a decision support system. Real time measurements and control actions are routed through the control center. A repository stores a collection of scenarios. Each scenario consists of: (a) a road network with fundamental diagrams, possibly uncertain, for all the links; (b) a set of forecasted demands, possibly uncertain, for all the origin links; (c) expected split ratios for all the nodes; (d) a set of controllers residing at some nodes; and (e) a set of events that change link parameters (e.g. capacities), split ratios, demands, or controller configurations at given times. For example, one Tuesday 8 AM event might specify a 2% increase in demand above the historical average, together with a random change of ± 100 vehicles per hour per lane in the capacity of each freeway link. A pair of events might specify an incident that begins at 8 AM and clears at 8:30 AM, and which reduces the capacity of the link with the incident by 50%. Controller sets with split ratio changing events describe control strategies. One strategy may consist of ALINEA ramp metering in a collection of ramps. Another strategy may consist of a changeable message sign that suggests a route around an incident. The latter strategy is modeled by a change in the split ratios. This repository would grow over time as new events and control strategies are considered. The ‘risk assessment’ box takes the best and worst cases of the state estimation and prediction algorithm and evaluates them according to various performance measures.

The decision support system would be used by the operator as follows. The state estimation block receives real time measurement and control information and continuously updates its current state estimate, following the algorithm of Section 5. The operator selects a time horizon τ , say 2 h, and one or more scenarios. Each scenario is executed by the prediction algorithm of Section 4. For each scenario, the operator examines the predicted best and worst case outcomes evaluated by the

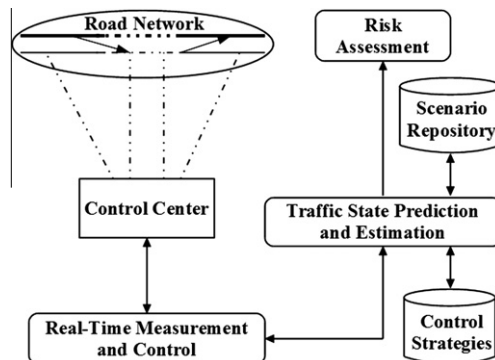


Fig. 8. Real time decision support system.

'risk assessment' block and determines whether the worst case outcome (a) poses such a small risk that the operator continues with the current control strategy; (b) poses significant risk, but in the operator's judgement the likelihood of this outcome is so small as to justify continuation with the current control strategy for the immediate future; or (c) poses such a high risk that the operator looks for a strategy in the repository that reduces the risk of the worst case outcome to an acceptable level.

In the absence of significant events, the operator would generally run scenarios, where no events are specified, only testing available control strategies for the forecasted demands. Large incidents, which have critical impact on the state of traffic are rare, and their time and location are unpredictable. When such an incident is reported, the operator can create a capacity reducing event at the location of the incident, and test a performance of various potential responses (i.e. controller sets in combination with split ratio changing events), as well as assess the impact of clearance time.

We simulate such a decision support system for the I-80 integrated corridor system, using a CTM model whose parameters are calibrated from I-80 data. This model is used in the 'traffic state estimation and prediction' block of Fig. 8. The 'risk assessment' block consists of various performance measures, including speed, delay and freeway productivity. The signals from the 'real time measurement and control' block are simulated using historical data rather than by actual 'real time' data. Thus the simulated system could be implemented in the I-80 corridor traffic management center, simply by replacing historical measurement data by actual data. We simulate two scenarios that the corridor operator may consider.

The first scenario concerns the 23 mile-long segment of eastbound I-80, from A (near the Oakland-San Francisco Bay Bridge) to B (near the Carquinez Bridge) in Fig. 9. I-80 eastbound is the afternoon commute direction. Traffic moves from post mile 3 to 27. Historical data for September 2, 2008, are used. The real time estimation algorithm provides the estimate of the state at 2 PM. At that time, the prediction algorithm is run for two hours, 2–4PM. The scenario specifies that the demand varies randomly between $\pm 2\%$ of nominal (which is taken to be the actual demand) and the capacity in each link varies randomly between $\pm 2\%$ of the calibrated capacity.

The plots on the top right in Fig. 9 predict the best and worst case speed profiles along the freeway segment at 3:30 PM under 'no control'. The plots show a large gap in these speeds between post miles 3 and 12, indicating the risk of congestion before 3:30 PM. The operator may find this risk unacceptable, and considers a congestion mitigation strategy that turns on an ALINEA control at three on-ramps between post miles 3 and 10. The plots on the lower right indicate that with this strategy the gap between worst and best case speed has been reduced between post miles 3 and 10. However, the risk of congestion

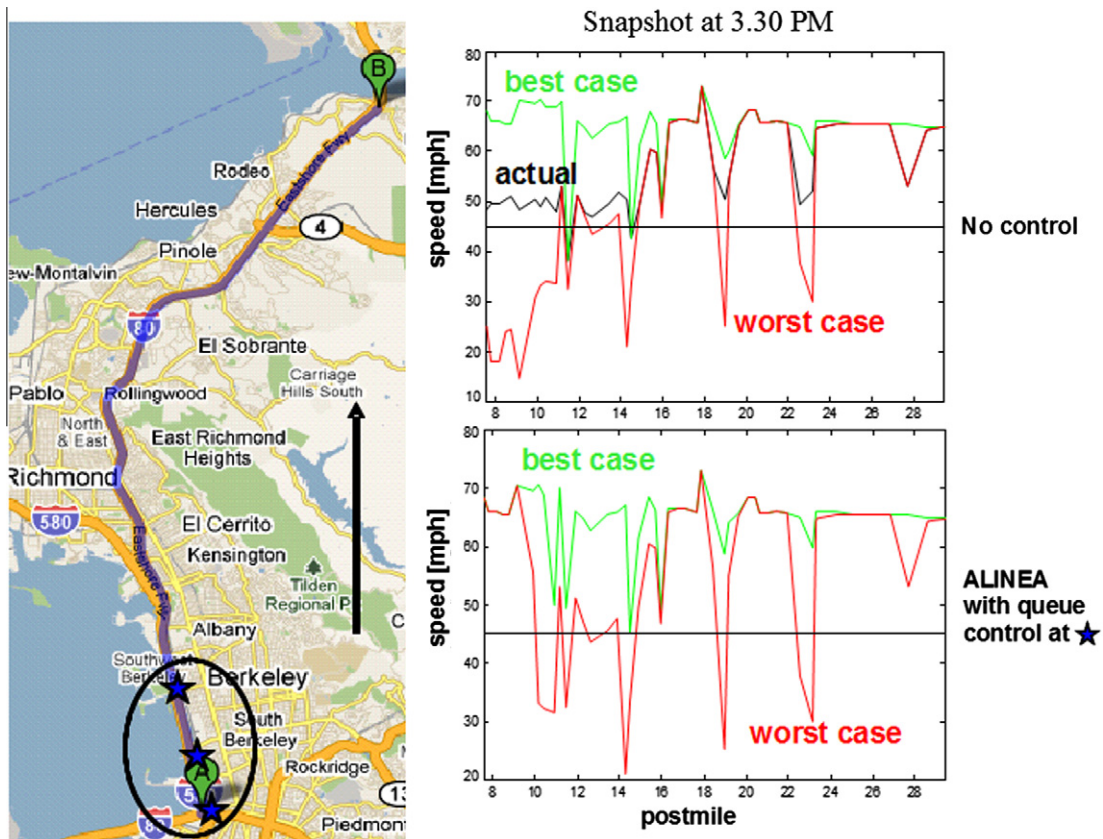


Fig. 9. Estimation and prediction for scenario 1.

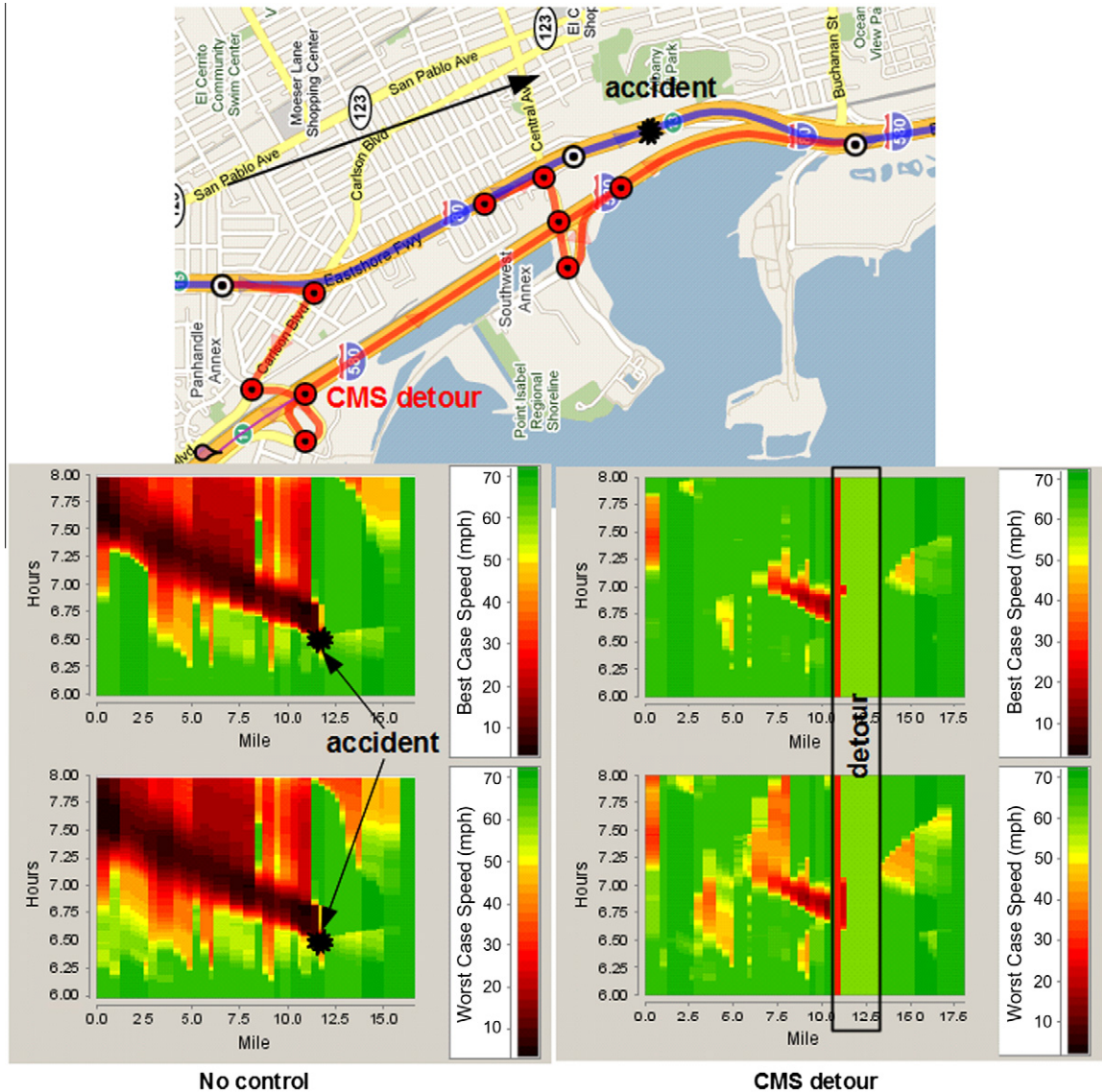


Fig. 10. Estimation and prediction for scenario 2.

further downstream is unchanged. The operator may conclude that the reduction in risk is sufficient to justify starting the ramp metering at 2 PM. The operator may decide to change the control strategy to consider the benefit of ramp metering further downstream.

The second scenario concerns the same segment of I-80, but in the westbound morning commute direction. Historical data for January 14, 2009 are used. The real time estimation algorithm estimates the traffic state at 6 AM, and the prediction algorithm is run for two hours, 6–8 AM. See Fig. 10. The scenario specifies the occurrence of an accident starting at 6:35 AM and clearing at 6:50 AM, which disables two (out of four) lanes. This is modeled as a 50% capacity reduction. The scenario further specifies that demand during 6–8 AM varies randomly between $\pm 2\%$ of nominal. The bottom left panel shows the speed contour plots (the horizontal axis represents post miles with traffic moving from left to right, the vertical axis represents time between 6 and 8 AM increasing from bottom to top, and color represents speed) for the best and worst cases under 'no control': in either case, the 15-min incident causes congestion to spread over 12 miles within 40 min. The operator decides to examine a strategy that combines ALINEA ramp metering upstream of the incident together with diversion of traffic around the incident by making use of the parallel westbound I-580 freeway. The road network was modified by adding two detour routes that overlap on I-580 and merge back into I-80 downstream of the incident, shown in red on the map. The diversion strategy is modeled as a change in the split ratio that diverts 10% of the traffic. The best and worst case speed contours for one of the detour routes (marked 'CMS detour' on the map) are shown in the bottom right panel; evidently

the extent of congestion has been reduced dramatically.⁹ Since historical data indicate that the link with the incident is an accident 'hot spot', the operator is more likely to decide to implement ALINEA control, but to hold back on diversion advice unless an actual accident is reported.

8. Conclusion

The paper presented an algorithm for guaranteed traffic state prediction and estimation of road networks described by a CTM model with uncertainty in demand, model parameters and measurement. The prediction and the estimate are in the form of sets of states that are guaranteed to include the actual state. The practical value of the proposed algorithm is its simple implementation. The only required data are the uncertainty ranges, which must be specified as intervals.

The algorithm calculates bounding curves $\rho^-(\cdot)$, $\rho^+(\cdot)$, which guarantee that any state trajectory $\rho(\cdot)$ of the original system satisfies $\rho^-(\cdot) \leq \rho(\cdot) \leq \rho^+(\cdot)$. The box-valued set $\Omega(t)$ described by its extreme points $\rho^-(\cdot)$ and $\rho^+(\cdot)$ is thus an overapproximation of the reachable set of the system (2.1)–(2.7), tight in the class of boxes. In one important special case (Theorem 4.3), however, the curves $\rho^-(\cdot)$, $\rho^+(\cdot)$ become trajectories of (2.1)–(2.7).

A link through which traffic enters the network can be controlled by an open- or closed-loop controller. The presence of the open-loop controller does not interfere with the prediction algorithm of Section 4 and, as mentioned in Section 6, may even make the system more predictable by tightening density bounds downstream of the controller. The impact of the closed-loop flow control is the same as that of the open-loop, when the system (4.1)–(4.17) is used in real time for state estimation. If, on the other hand, the system (4.1)–(4.17) is used just for prediction, the closed-loop controller produces an interval of potential flow rates, which is used in the input demand bound computation for (formulas (6.2) and (6.3) replace (4.4) and (4.5)).

The proposed method could be used in the following way. Several prediction algorithms with different pre-configured control strategies are run continuously by the traffic operator for a time horizon of 1–2 hours with initial conditions coming from estimation. Based on the prediction results, the operator chooses to deploy one control strategy or another. This choice may depend on how predictable the system is (the smaller the intervals between the worst and the best cases, the more predictable the system), how bad the worst case is on particular links, which strategy yields the smallest total delay, or some other criteria.

The algorithm described here is implemented in Aurora Road Network Modeler, an open source software package for macroscopic traffic simulation (Aurora RNM Homepage, n.d.). This software was used to illustrate how the algorithm can provide real time decision support to an operator managing the I-80 corridor in the San Francisco Bay Area.

Acknowledgements

This research was supported by National Science Foundation Award CMMI-0941326 and the California Department of Transportation. We are grateful to members of the TOPL research project (TOPL Project, n.d.), especially G. Derivisoglu, G. Gomes, R. Horowitz, A. Muralidharan and R. Sanchez. We would also like to thank the anonymous reviewers, whose meticulous reading and thoughtful comments helped improve this paper.

References

- Aurora RNM Homepage (n.d.). <<http://code.google.com/p/aurorarnm>>.
- Bliemer, M., 2007. Dynamic queueing and spillback in an analytical multiclass dynamic network loading model. *Transportation Research Record* (2029), 14–21.
- Chow, A.H.F., Gomes, G., Kurzhanskiy, A.A., Varaiya, P., 2010. Aurora RNM – a macroscopic tool for arterial traffic modeling and control. In: 89th Annual Meeting of the Transportation Research Board, Washington, DC, USA.
- Courant, R., Friedrichs, K., Lewy, H., 1928. 'Über die partiellen Differenzengleichungen der mathematischen Physik. *Mathematische Annalen* 100 (1), 32–74.
- Daganzo, C.F., 1994. The cell transmission model: a dynamic representation of highway traffic consistent with the hydrodynamic theory. *Transportation Research Part B* 28 (4), 269–287.
- Daganzo, C.F., 1995. The cell transmission model II: network traffic. *Transportation Research Part B* 29 (2), 79–93.
- Derivisoglu, G., Gomes, G., Kwon, J., Muralidharan, A., Varaiya, P., 2009. Automatic calibration of the fundamental diagram and empirical observations on capacity. In: 88th Annual Meeting of the Transportation Research Board, Washington, DC, USA.
- Gomes, G., Horowitz, R., Kurzhanskiy, A.A., Kwon, J., Varaiya, P., 2008. Behavior of the cell transmission model and effectiveness of ramp metering. *Transportation Research Part C* 16 (4), 485–513.
- Hegyi, A., Girimonte, D., Babuška, R., De Schutter, B., 2006. A comparison of filter configurations for freeway traffic state estimation. In: Proceedings of the IEEE ITSC Conference on Intelligent Transportation Systems, Toronto, Canada pp. 1029–1034.
- Jin, W., Zhang, H.M., 2003. On the distribution schemes for determining flows through a merge. *Transportation Research Part B* 37 (6), 521–540.
- Julier, S., Uhlmann, J., Durant-Whyte, H., 2000. A new method for the nonlinear transformation of means and covariances in filters and estimators. *IEEE Transactions on Automatic Control* 45 (3), 477–482.
- Kumar, P.R., Varaiya, P., 1986. *Stochastic Systems: Estimation, Identification and Adaptive Control*. Prentice-Hall.
- Kurzhanski, A.B., 1972. Differential games of observation. *Doklady Mathematics, Journal of the Academy of Sciences of the USSR* 13 (6), 1556–1560.
- Kurzhanski, A.B., 1989. Identification – a theory of guaranteed estimates. In: Willems, J.C. (Ed.), *From Data to Model*. Springer Verlag, pp. 135–214.
- Kurzhanskiy, A.A., 2009. Set-valued estimation of freeway traffic density. In: Proceedings of the 12th IFAC Symposium on Control in Transportation Systems.

⁹ The red stripe in the detour area of both the best and worst speed contours representing speed around 30 mph corresponds to the arterial segment of the detour route.

- Kurzhanskiy, A.A., Varaiya, P., 2010. Active traffic management on road networks: a macroscopic approach. *Philosophical Transactions of The Royal Society, Part A* 368, 4607–4626.
- Kurzhanskiy, A.A., Kwon, J., Varaiya, P., 2009. Aurora Road Network Modeler. *Proceedings of the 12th IFAC Symposium on Control in Transportation Systems*.
- Lebacque, J.-P., Khoshyaran, M.M., 2005. First order macroscopic traffic flow models: intersection modeling, network modeling. *Proceedings of the 16th International Symposium of Transportation and Traffic Theory (ISTTT)* pp. 365–386.
- Lin, W.H. 2001., Spillovers, merging traffic and the morning commute. In: *Proceedings of the 4th IEEE Intelligent Transportation Systems Conference, Oakland, CA*.
- Mihaylova, L., Boel, R., Hegyi, A., 2007. Freeway traffic estimation within particle filtering framework. *Automatica* 43, 290–300.
- Milanese, M., Norton, J., Piet-Lahanier, H., Walter, E., 1996. *Bounding Approaches to System Identification*. Springer Verlag.
- Muralidharan, A., Dervisoglu, G., Horowitz, R., 2011. Probabilistic graphical models of fundamental diagram parameters for freeway traffic simulations. In: *90th Annual Meeting of the Transportation Research Board, Washington, DC, USA*.
- Okutani, I., Stephanedes, Y.J., 1984. Dynamic prediction of traffic volume through kalman filtering theory. *Transportation Research Part B* 18, 1–11.
- Papageorgiou, M., Hadj-Salem, H., Blosseville, H.M., 1991. ALINEA: A local feedback control law for onramp metering. *Transportation Research Record. PeMS Homepage* (n.d.). <<http://pems.eecs.berkeley.edu>>.
- Smith, B.L., Williams, B.M., Oswald, R.K., 2002. Comparison of parametric and nonparametric models for traffic flow forecasting. *Transportation Research Part C* 10, 303–321.
- Sun, X., Muñoz, L., Horowitz, R., 2003. Highway Traffic State Estimation Using Improved Mixture Kalman Filters for Effective Ramp Metering Control. In: *Proceedings of the 42nd Conference on Decision and Control*, pp. 6333–6338.
- Tampère, C.M.J., Immers, L.H., 2007. An extended kalman filter application for traffic state estimation using CTM with implicit mode switching and dynamic parameters. In: *Proceedings of the 2007 IEEE Intelligent Transportation Systems Conference* pp. 209–216.
- Tampère, C.M.J., Corthout, R., Cattrysse, D., Immers, L.H., 2011. A generic class of first order node models for dynamic macroscopic simulation of traffic flows. *Transportation Research Part B* 45 (1), 289–309.
- TOPL Project (n.d.). <<http://path.berkeley.edu/topl>>.
- Wang, Y., Papageorgiou, M., 2007. Real-time freeway traffic state estimation based on extended kalman filter: a general approach. *Transportation Research Part B* 39 (2), 141–167.